2023 IEEE 66th International Midwest Symposium on Circuits and Systems (MWSCAS)
Phoenix, Arizona, USA, August 6-9, 2023

Single Photon LiDAR Compression: An Overview

Abdullah H Al-Shabili[1], Hashan K Weerasooriya[1], Harshana Weligampola[1], Prateek Chennuri[1],
Pamela Abshire[2], Stanley Chan[1]
[1]*School of Electrical and Computer Engineering*
Purdue University, West Lafayette, IN, USA
[2]*Department of Electrical and Computer Engineering and Institute of System Research*
University of Maryland, College Park, MD, USA
aalshabi@purdue.edu, hweeraso@purdue.edu, wweligam@purdue.edu, pchennur@purdue.edu,
pabshire@umd.edu, stanchan@purdue.edu

2023 IEEE 66th International Midwest Symposium on Circuits and Systems (MWSCAS) | 979-8-3503-0210-3/23/$31.00 ©2023 IEEE | DOI: 10.1109/MWSCAS57524.2023.10405954

***Abstract*—Real-time mapping of the surroundings plays a pivotal role in ensuring the success of autonomous vehicles. Among the technologies showing promise for depth mapping is Single Photon Light Detection and Ranging (SPL) which offers impressive long-range capabilities, superior depth resolution, and energy-efficient laser sources. However, the adoption of high-resolution, high frame-rate SPL systems results in significant data volumes, often reaching several Gbit/s. This creates a throughput bottleneck that impedes real-time applications and necessitates the development of effective compression schemes. This paper addresses the challenges associated with SPL compression and provides a comprehensive overview of recent advancements in this domain. The review encompasses various compression methods, including algorithmic and/or hardware-based approaches, spatial and/or temporal compression techniques. We also discuss future directions, such as integrating deep learning and fusion techniques with other sensing modalities.**

***Index Terms*—Single Photon LiDAR (SPL), compression, depth imaging, deep learning, compressive learning, compressive sensing.**

I. Introduction

Accurately mapping and responding to surroundings in real-time is crucial for the success of autonomous vehicles, making SPL a promising technology for depth mapping due to its long-range capabilities, excellent depth resolution, and low-power laser sources [1]–[4]. However, the remarkable sensitivity of single-photon detectors introduces challenges such as noise modeling [5] and managing the massive data throughput [6]. This article focuses on the latter issue by reviewing and analyzing the current state of LiDAR compression methods.

SPL is composed of two sub-systems: the laser rangefinder system and the scanning or beam-steering system. The laser rangefinder system, illustrated in Figure 1, emits a pulse signal using a laser transmitter, which is reflected back from objects to a signal photon detector such as the Single-Photon Avalanche Diode (SPAD) photodetector. However, due to electronic timing uncertainty and photons from the background and ambient light sources, the process is repeated several times for each pixel. Time-Correlated Single-Photon Counting (TCSPC) is then, used to generate a time of flight (ToF) histogram, which is used to estimate the depth and reflectivity of objects. Meanwhile, the scanning system, such as mechanical spinning, flash, or optical phased array, is responsible for steering the beams to explore a larger area and achieve spatial resolution. By the end of the SPL system, a massive LiDAR data cube, usually hundreds of Gigabyte (GB) per second, consisting of a histogram per pixel is produced, which poses a significant challenge for real-time applications [6]–[8]. To address this challenge, algorithmic and hardware compression of SPL measurement is necessary.

This work was supported in part by COGNISENSE, one of seven centers in JUMP 2.0, a Semiconductor Research Corporation (SRC) program sponsored by DARPA.

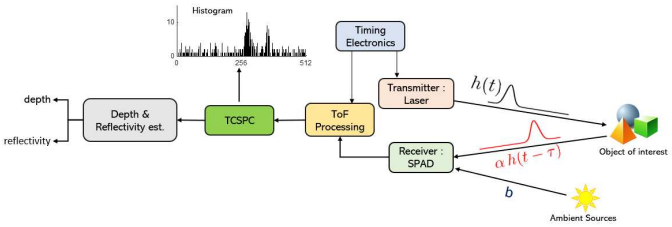

Fig. 1: LiDAR rangefinder system conceptual diagram.

To overcome the massive LiDAR data challenge, algorithmic and hardware compression is necessary. Different compression methods involving trade-offs between compression ratio, information loss, and computational complexity need to be carefully evaluated based on the specific application requirements. This article aims to review and analyze the current state of LiDAR compression methods to provide insights into their effectiveness, limitations, and potential for future development.

II. SPL Background

A. SPL Raw Data

In the SPL system, the SPAD sensor array with spatial dimension of $M \times N$ collaborates with timing electronics to produce ToF timestamps for each laser pulse. These ToF timestamps are subsequently processed using the TCSPC technique, resulting in a ToF histogram for each pixel. Raw data from the system may exist in two forms: a timestamp cube $\tilde{\mathbf{y}} \in \mathbb{R}^{M\times N\times p}$, where p represents the number of timestamps, or more commonly a histogram cube $\mathbf{y} \in \mathbb{R}^{M\times N\times d}$, where d denotes the histogram resolution determined by the number of

TABLE I: LiDAR Compression Literature*

Author (Year)	Method	Description	TC	SC
Henderson et al. [9], [10] (2018-19)	Coarse	Hardware solution: a gated procedure to compute a coarse histogram.	✓	
Ren et al. [11](2018)	Coarse	Hardware solution: a sliding detector gate to achieve high-resolution depth.	✓	✓
Gyongy et al. [12] (2020)	Coarse	Hardware solution: coarse histogram with wide pulse for better depth resolution.	✓	
Della Rocca et al. [13], [14] (2019-20)	Coarse & Activity	Hardware solution: only collect measurements based on activity changes.		
Hutchings et al. [15] (2019)	Coarse & Activity	Hardware solution: discard photon detections based on activity.		
Zhang et al. [16] (2018)	Coarse-to-fine	Hardware solution: a coarse to fine approximation of the ToF data.		
Rapp et al. [17], [18] (2018-20)	Coarse & dithering	Hybrid solution: solution: coarse histogram followed by subtractive dithering for higher depth resolution.	✓	
Kadambi and Boufounos [19] (2015)	Compressive sensing	Algorithmic solution: use coded aperture with compressed sensing to improve spatial resolution.	✗	✓
Halimi et al., [20] (2019)	Adaptive sampling	Algorithmic solution: scene-dependent adaptive sampling approach by iteratively focusing on interest regions and reducing the acquisition time.	✗	✓
Bergman et al. [21] (2020)	Adaptive sampling	Algorithmic solution: adaptive sampling based on an end-to-end deep learning-based depth completion algorithms.		
Zhang et al. [22] (2022)	First arrival differential	Hybrid solution: record a temporal differential measurement between pairs of pixels followed by depth reconstruction algorithm.	✓	✓
Sheehan et al. [8] (2021)	Compressive learning	Algorithmic solution: follow compressive learning by sampling the characteristic function of the ToF model to obtain a compressive statistic of the histogram sufficient for depth and distance and intensity estimation.	✓	✗
Tachella et al. [23] (2022)	Compressive learning	Algorithmic solution: similar to [8] with additional penalty to capture spatial correlation.	✓	✓
Sheehan et al. [24] (2022)	Compressive learning	Algorithmic solution: an extension of [8] using piece-wise polynomial splines to form a hardware-friendly compressed statistic.	✓	✗
Gutierrez-Barragan et al. [25] (2022)	Linear coding	Algorithmic solution: on-the-fly linear compression of the detected photons to form a compressed histogram.	✓	✗
Poisson et al. [26] (2022)	Linear coding & deep learning recovery	Algorithmic solution: compute ToF histogram compressive sensing (CS) with a deep generative model reconstruction.	✓	✓

* TC and SC stand for Temporal and Spatial Compression, respectively.

bins. While the conversion between the two formats is algorithmically simple, the selection of using either the timestamp cube or the histogram cube depends on factors such as noise level and the ratio of timestamps to the histogram resolution. Ultimately, the data cube is processed to estimate the depth and reflectivity of the scene. However, in high-resolution and high-frame-rate scenarios, the significant volume of data generated by the SPL system can pose challenges for real-time applications.

B. SPL Observation Model

The photon counts measured for each pixel, assuming a single depth per pixel [5], [27]–[31], are represented by a Poisson distribution:

$$\mathbf{y}_{i,j} = \text{Poisson}\left(\alpha_{i,j}\, h(t - \tau_{i,j}) + b\right) \tag{1}$$

Here, $\mathbf{y}_{i,j}$ refers to the i^{th} and j^{th} pixel of the data cube $\mathbf{y}$. The parameter $0 \leq \alpha_{i,j} \leq 1$ represents the surface reflectivity, $h(t)$ represents the pulse shape, $\tau_{i,j}$ represents the ToF, and b represents the background noise originating from ambient light or dark counts. To maintain clarity, the pixel index will be omitted unless specifically needed. In synthetic examples, a Gaussian pulse shape is assumed, but in practical settings, the pulse shape is empirically measured. Furthermore, this model can be extended to accommodate scenarios involving multiple depths per pixel [32]–[36].

Alternatively, the timestamps cube $\tilde{\mathbf{y}}$ can be modeled as a mixture model. For instance, [37] models the detected photon timestamp Probability Mass Function (PMF) as:

$$\pi(\tilde{\mathbf{y}} \mid \rho, \tau) = \rho\, \pi_s(\tilde{\mathbf{y}} \mid \tau) + (1 - \rho)\, \pi_b(\tilde{\mathbf{y}}), \tag{2}$$

Here, ρ represents the mixture model weight, while π_s and π_b denote the PMF of signal and background detected photon timestamps, respectively. The signal component is proportional to the transmitted pulse, while the background component is typically modeled as a discrete uniform distribution

III. SPL Compression Methods Taxonomy

In this section, we delve into the topic of compression methods that effectively address the data deluge challenge in SPL. To better understand and classify these compression methods, we consider various aspects, including spatial and/or temporal techniques, as well as hardware and/or algorithmic approaches. To provide an overview of the existing literature on LiDAR compression, we present Table I, which summarizes key references in the field. Subsequently, we delve into several compression methods that represent the main themes in SPL compression.

A. Coarse Histogram

One approach to compression is to balance the computational resources and depth resolution by employing a coarse histogram [9], [10]. This method involves using a smaller value of d in the SPL data cube $\mathbf{y}$, thereby reducing memory requirements at the expense of sacrificing depth accuracy. A similar implementation where adjacent pixels are merged to get a single output can also be applied to the spatial dimensions. While this approach is straightforward to implement in hardware, it does not yield substantial compression ratios. To overcome the coarse histogram disadvantages, [16] proposed a coarse-to-fine approach. Also, [17], [18] investigated subtractive dithering to improve the depth resolution without increasing the temporal resolution.

B. Linear Compression

Focusing on a single pixel, recall that SPL system measure timestamps $\tilde{y} \in \mathbb{R}$, that are then converted into a histogram $\mathbf{y} \in \mathbb{R}^d$. The conversion is achieved by summing up one-hot coding vectors, denoted as $\mathbf{e}(\tilde{y})$, for each timestamp:

$$\mathbf{y} = \sum_{i=1}^{p} \mathbf{e}(\tilde{y}). \tag{3}$$

To compress this histogram representation while retaining important information, a technique called linearly compressed histogram was proposed by [25]. It involves using a coding matrix, denoted as $\mathbf{C}$, with dimensions $m \times d$, where m is significantly smaller than d. The compressed histogram can be obtained as:

$$\mathbf{g} = \sum_{i=1}^{p} \mathbf{C}\, \mathbf{e}(\tilde{y}). \tag{4}$$

By employing this linear compression, it becomes possible to represent the original histogram more efficiently, effectively reducing its dimensions. This approach provides flexibility, as the linearly compressed histogram offers various instances depending on the chosen coding matrix. Notable examples of these instances include:

- Classical histogram: Utilizing an identity coding matrix and recovers (3),
- Coarse histogram: Employing a downsampling coding matrix that implements block summing,
- Truncated discrete Fourier transform (T-DFT): A composition of two linear operators, namely the downsampling and DFT.

The selection of the coding matrix depends on factors such as scene complexity, pulse shape, and noise level. For instance, when assuming a Gaussian pulse, T-DFT is suitable as it captures most of the low frequencies.

After the linear compression stage, the compressed representation $\mathbf{g}$ is processed by a decoder to infer depths. [25] proposed a simple correlation-based decoding method:

$$\widehat{\tau} = \arg\max_{i} \mathbf{C}_{:,i}^{T}\, \mathbf{g}. \tag{5}$$

In the decoding stage, the decoder seeks the column of the coding matrix that exhibits the highest correlation with the compressed histogram. The linear compression approach, implemented by the simple encoder, offers a balance between simplicity and compression ratio. However, it is important to note that the current discussion of linear compression has been confined to the temporal dimension. To achieve even higher compression ratios, it becomes imperative to explore spatial-temporal redundancies.

C. Compressive Learning

The Compressive Learning (CL) framework leverages a nonlinear feature mapping and averaging to generate a lower-dimensional representation, termed a sketch, of SPL timestamps. This sketch is computed as:

$$\mathbf{g} = \frac{1}{p} \sum_{i=1}^{p} \Phi(\tilde{y}) \tag{6}$$

where $\Phi : \mathbb{R} \to \mathbb{R}^m$ is a nonlinear feature map, and m is significantly smaller than the total number of timestamps, p. It is noteworthy that the linear compression method can be seen as a specific case within the broader CL framework.

Additionally, the sketch can be interpreted from a statistical viewpoint as generalized moments. To see that, note that as the number of detected timestamps, p, tends to infinity, the sketch approaches the expected value $\mathbb{E}\{\tilde{y}\}$ due to the strong law of large numbers. The choice of the feature map leads to the recovery of classical probability concepts including:

- The k^{th} moment: $\mathbb{E}\{\tilde{y}^k\}$ where $\Phi(\tilde{y}) = \tilde{y}^k$,
- Characteristic function (CF): $\Psi(\omega) = \mathbb{E}\{e^{j\omega\tilde{y}}\}$ where $\Phi(\tilde{y}) = e^{j\omega\tilde{y}}$ and ω denotes the frequency.

Assuming the closed-form existence of $\mathbb{E}\{\tilde{y}\}$, which is only valid under simple distributions of $\tilde{y}$ and specific feature maps Φ, the decoder stage aims to estimate the depth and reflectivity by minimizing the distance between the sketch and the closed-form expectation:

$$\widehat{\alpha}, \widehat{\tau} = \arg\min_{\alpha,\tau} \left\| \frac{1}{p} \sum_{i=1}^{p} \Phi(\tilde{y}) - \mathbb{E}_{\alpha,\tau}\{\tilde{y}\} \right\|^2, \tag{7}$$

where $\widehat{\alpha}$ and $\widehat{\tau}$ represent the estimated depth and reflectivity, respectively. This non-convex optimization problem is solved iteratively to obtain accurate estimates.

In [8], [38], the compressive learning (CL) framework was applied to SPL using the ToF mixture model (2). The authors employed the CL framework by utilizing a complex exponential feature map, denoted as Φ. Consequently, the resulting sketch can be interpreted as an empirical approximation of the Fourier transform of the density function associated with the SPL timestamps. It is worth noting that this specific choice of the feature map is equivalent to linear compression with a DFT and downsampling coding matrix. However, the distinction lies in the decoder stage. The CL framework is limited by the requirement of a closed-form expression for the expected value, which is only available for simple feature mapping. This limitation affects the achievable compression ratio.

The discussion so far has focused on exploiting temporal correlation. In [8], spatial correlation was exploited by adding a penalty term that models the spatial correlation between pixel depths and reflectivity. The penalty is implemented through a PnP (Plug-and-Play) approach called RT3D [35].

D. Compressive Sensing

Compressive Sensing (CS) is a technique that aims to decrease the data acquisition rate by capturing a limited number of linear measurements and employing reconstruction algorithms that leverage the inherent structure of the underlying signal, such as sparsity. In [19], the utilization of a coded aperture was suggested to acquire these linear measurements using a smaller sensor array. Subsequently, depth reconstruction algorithms were employed to restore a higher-resolution depth map. It should be noted, however, that in the aforementioned example, CS solely exploits spatial redundancy and does not take into account the temporal aspect.

E. Adaptive Sampling

The objective of the adaptive sampling approach is to reduce memory demand by selectively collecting measurements based on a specific metric. The authors in [13]–[15] proposed adaptive sampling based on significant changes in the activity of the scene. This technique minimizes the amount of data being transferred since it is only necessary in specific instances. However, it is important to note that these approaches may remain inactive in situations where there is only a slight alteration in activity. In a similar vein, [20] proposed enhancing sampling by utilizing depth image statistics to create a map of important areas. This map influences the choice of sample positions and acquisition timing. It is worth noting that while adaptive sampling reduces memory demand, it often comes at the cost of additional computational overhead for real-time applications.

F. Deep Learning Methods

Deep Learning (DL) has made significant advancements in addressing various conventional challenges in image processing and computer vision. Notably, there is an observable surge in the adoption of DL techniques for SPL compression. In [26], the authors introduced an end-to-end encoder-decoder neural network architecture. The encoder module employs one-hot coding, followed by a random linear transformation sampled from the Rademacher distribution. On the other hand, the decoder module utilizes a deep generative model that has been trained to accurately reconstruct both the depth and reflectivity attributes. In [21], the authors proposed adaptive sampling for depth completion at low sampling rates. The proposed system exhibits differentiability, enabling seamless end-to-end training of both the sparse depth sampling and depth inpainting components. The authors' work highlights the significance of adaptive sampling.

IV. Conclusion

In conclusion, this paper emphasizes the significance of real-time mapping for autonomous vehicles. Single Photon Light Detection and Ranging (SPL) technology offers impressive long-range capabilities and superior depth resolution but generates substantial data volumes, creating a throughput bottleneck. The paper addresses SPL compression challenges, provides a comprehensive overview of recent advancements, and discusses various compression methods, including algorithmic and hardware-based approaches. Looking ahead, the expansion of SPL's capabilities will involve the utilization of multiple wavelengths, thereby increasing the importance of addressing the compression challenge. One promising direction is to optimize lidar acquisition resources and fuse additional information from other sensing modalities, such as standard red–green–blue images and radar. Deep neural networks are anticipated to play a significant role in SPL compression by exploring spatial-temporal redundancies and facilitating the fusion of diverse modalities. By overcoming compression challenges and leveraging emerging technologies, SPL can greatly advance real-time mapping for autonomous vehicles.

References

[1] B. Behroozpour, P. A. Sandborn, M. C. Wu, and B. E. Boser, "Lidar system architectures and circuits," *IEEE Communications Magazine*, vol. 55, no. 10, pp. 135–142, 2017.

[2] Y. Li and J. Ibanez-Guzman, "Lidar for autonomous driving: The principles, challenges, and trends for automotive lidar and perception systems," *IEEE Signal Processing Magazine*, vol. 37, no. 4, pp. 50–61, 2020.

[3] J. Rapp, J. Tachella, Y. Altmann, S. McLaughlin, and V. K. Goyal, "Advances in single-photon lidar for autonomous vehicles: Working principles, challenges, and recent advances," *IEEE Signal Processing Magazine*, vol. 37, no. 4, pp. 62–71, 2020.

[4] J. Nubert, S. Khattak, and M. Hutter, "Self-supervised learning of lidar odometry for robotic applications," in *2021 IEEE International Conference on Robotics and Automation (ICRA)*, pp. 9601–9607, IEEE, 2021.

[5] D. Shin, A. Kirmani, V. K. Goyal, and J. H. Shapiro, "Photon-efficient computational 3-d and reflectivity imaging with single-photon detectors," *IEEE Transactions on Computational Imaging*, vol. 1, no. 2, pp. 112–125, 2015.

[6] I. Maksymova, C. Steger, and N. Druml, "Review of lidar sensor data acquisition and compression for automotive applications," *Multidisciplinary Digital Publishing Institute Proceedings*, vol. 2, no. 13, p. 852, 2018.

[7] R. J. Walker, J. A. Richardson, and R. K. Henderson, "A 128×96 pixel event-driven phase-domain $\delta\sigma$-based fully digital 3d camera in $0.13\mu m$ cmos imaging technology," in *2011 IEEE International Solid-State Circuits Conference*, pp. 410–412, 2011.

[8] M. P. Sheehan, J. Tachella, and M. E. Davies, "A sketching framework for reduced data transfer in photon counting lidar," *IEEE Transactions on Computational Imaging*, vol. 7, pp. 989–1004, 2021.

[9] R. K. Henderson, N. Johnston, H. Chen, D. D.-U. Li, G. Hungerford, R. Hirsch, D. McLoskey, P. Yip, and D. J. Birch, "A 192 × 128 time correlated single photon counting imager in 40nm cmos technology," in *ESSCIRC 2018-IEEE 44th European Solid State Circuits Conference (ESSCIRC)*, pp. 54–57, IEEE, 2018.

[10] R. K. Henderson, N. Johnston, S. W. Hutchings, I. Gyongy, T. Al Abbas, N. Dutton, M. Tyler, S. Chan, and J. Leach, "5.7 a 256× 256 40nm/90nm cmos 3d-stacked 120db dynamic-range reconfigurable time-resolved spad imager," in *2019 IEEE International Solid-State Circuits Conference-(ISSCC)*, pp. 106–108, IEEE, 2019.

[11] X. Ren, P. W. Connolly, A. Halimi, Y. Altmann, S. McLaughlin, I. Gyongy, R. K. Henderson, and G. S. Buller, "High-resolution depth profiling using a range-gated cmos spad quanta image sensor," *Optics express*, vol. 26, no. 5, pp. 5541–5557, 2018.

[12] I. Gyongy, S. W. Hutchings, A. Halimi, M. Tyler, S. Chan, F. Zhu, S. McLaughlin, R. K. Henderson, and J. Leach, "High-speed 3d sensing via hybrid-mode imaging and guided upsampling," *Optica*, vol. 7, no. 10, pp. 1253–1260, 2020.

[13] F. M. Della Rocca, H. Mai, S. W. Hutchings, T. Al Abbas, A. Tsiamis, P. Lomax, I. Gyongy, N. A. Dutton, and R. K. Henderson, "A 128× 128 spad dynamic vision-triggered time of flight imager," in *ESSCIRC 2019-IEEE 45th European Solid State Circuits Conference (ESSCIRC)*, pp. 93–96, IEEE, 2019.

[14] F. M. Della Rocca, H. Mai, S. W. Hutchings, T. Al Abbas, K. Buckbee, A. Tsiamis, P. Lomax, I. Gyongy, N. A. Dutton, and R. K. Henderson, "A 128× 128 spad motion-triggered time-of-flight image sensor with in-pixel histogram and column-parallel vision processor," *IEEE Journal of Solid-State Circuits*, vol. 55, no. 7, pp. 1762–1775, 2020.

[15] S. W. Hutchings, N. Johnston, I. Gyongy, T. Al Abbas, N. A. Dutton, M. Tyler, S. Chan, J. Leach, and R. K. Henderson, "A reconfigurable 3-d-stacked spad imager with in-pixel histogramming for flash lidar or high-speed time-of-flight imaging," *IEEE Journal of Solid-State Circuits*, vol. 54, no. 11, pp. 2947–2956, 2019.

[16] C. Zhang, S. Lindner, I. M. Antolović, J. M. Pavia, M. Wolf, and E. Charbon, "A 30-frames/s, 252×144 spad flash lidar with 1728 dual-clock 48.8-ps tdcs, and pixel-wise integrated histogramming," *IEEE Journal of Solid-State Circuits*, vol. 54, no. 4, pp. 1137–1151, 2018.

[17] J. Rapp, R. M. Dawson, and V. K. Goyal, "Improving lidar depth resolution with dither," in *2018 25th IEEE International Conference on Image Processing (ICIP)*, pp. 1553–1557, IEEE, 2018.

[18] J. Rapp, R. M. Dawson, and V. K. Goyal, "Dithered depth imaging," *Optics Express*, vol. 28, no. 23, pp. 35143–35157, 2020.

[19] A. Kadambi and P. T. Boufounos, "Coded aperture compressive 3-d lidar," in *2015 IEEE International Conference on Acoustics, Speech and Signal Processing (ICASSP)*, pp. 1166–1170, IEEE, 2015.

[20] A. Halimi, P. Ciuciu, A. Mccarthy, S. Mclaughlin, and G. S. Buller, "Fast adaptive scene sampling for single-photon 3d lidar images," in *2019 IEEE 8th International Workshop on Computational Advances in Multi-Sensor Adaptive Processing (CAMSAP)*, pp. 196–200, IEEE, 2019.

[21] A. W. Bergman, D. B. Lindell, and G. Wetzstein, "Deep adaptive lidar: End-to-end optimization of sampling and depth completion at low sampling rates," in *2020 IEEE International Conference on Computational Photography (ICCP)*, pp. 1–11, IEEE, 2020.

[22] T. Zhang, M. J. White, A. Dave, S. Ghajari, A. Raghuram, A. C. Molnar, and A. Veeraraghavan, "First arrival differential lidar," in *2022 IEEE International Conference on Computational Photography (ICCP)*, pp. 1–12, IEEE, 2022.

[23] J. Tachella, M. P. Sheehan, and M. E. Davies, "Sketched rt3d: How to reconstruct billions of photons per second," in *ICASSP 2022-2022 IEEE International Conference on Acoustics, Speech and Signal Processing (ICASSP)*, pp. 1566–1570, IEEE, 2022.

[24] M. P. Sheehan, J. Tachella, and M. E. Davies, "Spline sketches: An efficient approach for photon counting lidar," *arXiv preprint arXiv:2210.07314*, 2022.

[25] F. Gutierrez-Barragan, A. Ingle, T. Seets, M. Gupta, and A. Velten, "Compressive single-photon 3d cameras," in *Proceedings of the IEEE/CVF Conference on Computer Vision and Pattern Recognition*, pp. 17854–17864, 2022.

[26] V. Poisson, W. Guicquero, G. Sicard, *et al.*, "Luminance-depth reconstruction from compressed time-of-flight histograms," *IEEE Transactions on Computational Imaging*, vol. 8, pp. 148–161, 2022.

[27] D. Shin, J. H. Shapiro, and V. K. Goyal, "Single-photon depth imaging using a union-of-subspaces model," *IEEE Signal Processing Letters*, vol. 22, no. 12, pp. 2254–2258, 2015.

[28] Y. Altmann, X. Ren, A. McCarthy, G. S. Buller, and S. McLaughlin, "Lidar waveform-based analysis of depth images constructed using sparse single-photon data," *IEEE Transactions on Image Processing*, vol. 25, no. 5, pp. 1935–1946, 2016.

[29] J. Rapp and V. K. Goyal, "A few photons among many: Unmixing signal and noise for photon-efficient active imaging," *IEEE Transactions on Computational Imaging*, vol. 3, no. 3, pp. 445–459, 2017.

[30] F. Heide, S. Diamond, D. B. Lindell, and G. Wetzstein, "Sub-picosecond photon-efficient 3d imaging using single-photon sensors," *Scientific reports*, vol. 8, no. 1, pp. 1–8, 2018.

[31] J. Koo, A. Halimi, and S. McLaughlin, "A bayesian based deep unrolling algorithm for single-photon lidar systems," *arXiv preprint arXiv:2201.10910*, 2022.

[32] S. Hernandez-Marin, A. M. Wallace, and G. J. Gibson, "Bayesian analysis of lidar signals with multiple returns," *IEEE Transactions on Pattern Analysis and Machine Intelligence*, vol. 29, no. 12, pp. 2170–2180, 2007.

[33] D. Shin, F. Xu, F. N. Wong, J. H. Shapiro, and V. K. Goyal, "Computational multi-depth single-photon imaging," *Optics express*, vol. 24, no. 3, pp. 1873–1888, 2016.

[34] A. Halimi, R. Tobin, A. McCarthy, S. McLaughlin, and G. S. Buller, "Restoration of multilayered single-photon 3d lidar images," in *2017 25th European Signal Processing Conference (EUSIPCO)*, pp. 708–712, IEEE, 2017.

[35] J. Tachella, Y. Altmann, N. Mellado, A. McCarthy, R. Tobin, G. S. Buller, J.-Y. Tourneret, and S. McLaughlin, "Real-time 3d reconstruction from single-photon lidar data using plug-and-play point cloud denoisers," *Nature communications*, vol. 10, no. 1, pp. 1–6, 2019.

[36] A. Halimi, R. Tobin, A. McCarthy, J. Bioucas-Dias, S. McLaughlin, and G. S. Buller, "Robust restoration of sparse multidimensional single-photon lidar images," *IEEE Transactions on Computational Imaging*, vol. 6, pp. 138–152, 2019.

[37] Y. Altmann and S. McLaughlin, "Range estimation from single-photon lidar data using a stochastic em approach," in *2018 26th European Signal Processing Conference (EUSIPCO)*, pp. 1112–1116, IEEE, 2018.

[38] M. P. Sheehan, J. Tachella, and M. E. Davies, "Surface detection for sketched single photon lidar," in *2021 29th European Signal Processing Conference (EUSIPCO)*, pp. 621–625, IEEE, 2021.